Wright State University

CORE Scholar

2011

Aerosol Jet Printing of LSCF-CGO Cathode for Solid Oxide Fuel Cells

Paul Gardner
Wright State University

Follow this and additional works at: https://corescholar.libraries.wright.edu/etd_all

Part of the Chemistry Commons

Repository Citation

AEROSOL JET PRINTING OF LSCF-CGO CATHODE FOR SOLID OXIDE FUEL
CELLS

A thesis submitted in partial fulfillment
of the requirements for the degree of
Master of Science

By

Paul Michael Gardner
B.S., Ohio State University, 2008

2011
Wright State University

WRIGHT STATE UNIVERSITY

SCHOOL OF GRADUATE STUDIES

<u>September 12, 2011</u>

I HEREBY RECOMMEND THAT THE THESIS PREPARED UNDER
MY SUPERVISION BY <u>Paul Michael Gardner</u> ENTITLED <u>Aerosol Jet
Printing of LSCF-CGO Cathode for Solid Oxide Fuel Cells</u> BE ACCEPTED
IN PARTIAL FULFILLMENT OF THE REQUIREMENTS FOR THE
DEGREE OF <u>Master of Science</u>

_____
Eric Fossum, Ph.D.
Thesis Director

_____
Kenneth Turnbull, Ph.D.,
Chair, Department of Chemistry
College of Science and Mathematics

Committee on Final Examination

_____
Eric Fossum, Ph.D.

_____
David Grossie, Ph.D.

_____
Rachel Aga, Ph.D.

_____
Andrew Hsu, Ph.D.
Dean, School of Graduate Studies

ABSTRACT

Gardner, Paul Michael. Department of Chemistry, Wright State University, 2011.
Aerosol Jet Printing of LSCF-CGO Cathode for Solid Oxide Fuel Cells.

Solid oxide fuel cell (SOFC) technology has attracted great attention due to advantages such as low emissions and high efficiency. In this work, solid oxide fuel cells were fabricated by incorporating functional layers deposited by a novel aerosol jet® printing method. The buffer and cathode layers were printed from gadolinium doped ceria $(Ce_{0.9}Gd_{0.1})O_{1.95}$ (CGO) and $La_{0.6}Sr_{0.4}Co_{0.2}Fe_{0.8}O_{3-x}$ (LSCF) inks, respectively. The CGO layer was deposited on the sintered electrolyte and then LSCF was subsequently deposited onto the CGO layer. The polarization curves showed a 19% improvement in current density using LSCF as the cathode instead of LSM. Cathode grain size was shown to change by 85% over the sintering temperatures examined. Lastly, the effect that ethyl cellulose additive had on the resulting cathode was determined. It was discovered that the porosity of the microstructure was not correlated to the additive's molecular weight. The actual causes of the cathode porosity may be the order of polymer branching or the ethoxy content of the ethyl cellulose.

Table of Contents

List of Figures

List of Tables

Acknowledgement

Dedication

To my family and friends.

1. Introduction

Solid oxide fuel cell (SOFC) technology has attracted great attention due to its low emissions and high efficiency. Fuel cells are comprised of anode, electrolyte, and cathode layers. Common materials used in a SOFC are a composite of nickel oxide and 8 mol % yttria-stabilized zirconia (YSZ) , 8 mol % YSZ by itself, and the perovskite $La_{1-x}Sr_xMnO_3$ (LSM) for the anode, electrolyte, and cathode layers, respectively. The anode and cathode layers are designed to be porous and allow the passage of reactant gases such as hydrogen fuel and oxygen while the electrolyte is designed to be dense for electronic insulation. The criteria for anode and cathode material selection include high electronic and ionic conducting capabilities for increased fuel cell performance.

One of the main drawbacks of SOFCs is the high temperature necessary for operation, which increases costs and longer fuel cell start-up times. Therefore, efforts are underway to lower the operating temperature while maintaining reasonable performance characteristics. Operating temperatures of approximately 700 °C make it possible to use cheaper materials, reduce fuel cell degradation, and improve SOFC lifetime.[1] To improve upon existing cathodes, such as the perovskite $La_{1-x}Sr_xMnO_3$ (LSM), materials with higher electronic conductivity, oxygen ion conductivity, and a high oxygen surface exchange coefficient for faster kinetics at the gas/cathode interface are required.[2] For these reasons, $La_{0.6}Sr_{0.4}Co_{0.2}Fe_{0.8}O_{3x}$ (LSCF) was chosen as a cathode material to use. The disadvantage of using LSCF is the formation of undesirable byproducts such as the perovskite $SrZrO_3$ or lanthanum diffusion into the electrolyte from the cathode

1

microstructure. To resolve this, a buffer interlayer of $(Ce_{0.9}Gd_{0.1})O_{1.95}$ (CGO) is used between the cathode and electrolyte layers.

Conventional methods of SOFC fabrication include ceramic wet methods such as screen-printing, tape casting, slurry coating, slip casting, and tape calendaring.[3] These methods are simple compared to other methods, but there are difficulties in accurately controlling the microstructure and thickness. An alternative approach is data driven direct-write methods such as ink jet and aerosol jet deposition techniques (AJDT).[3] These methods have the advantages of precise control over microstructure, patterning, and layer thickness. Additionally, the computer controlled fabrication system allows for highly reproducible SOFC fabrication compared to other methods.

However, the aerosol jet deposition technique has not been applied to LSCF cathodes or the CGO buffer interlayer before to create an intermediate temperature SOFC. In this paper, characterization of SOFCs fabricated using the novel aerosol jet deposition technique with LSCF as the cathode and CGO as the buffer interlayer will be examined. Also, the microstructure of the cathode will be altered to produce a porous or a dense layer through: the parameters of the deposition technique, cathode sintering temperature, and ethyl cellulose additive.

2. Literature Review

2.1 Hydrogen Fuel Cells

Fuel cells convert energy from a fuel source into electricity by the two chemical half-reactions listed below at the interfaces between the anode, electrolyte, and cathode, in this case using hydrogen as the fuel and oxygen as the oxidant:

$$\text{Anode half-reaction: } H_2 \rightarrow 2\ H^+ + 2\ e^-$$

$$\text{Cathode half-reaction: } \tfrac{1}{2}\ O_2 + 2\ e^- + 2\ H^+ \rightarrow H_2O$$

$$\text{Overall reaction: } H_2 + \tfrac{1}{2}\ O_2 \rightarrow H_2O$$
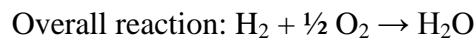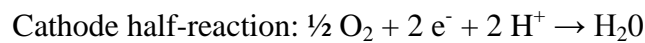
Multiple types of hydrogen fuel cells exist but they operate in a similar manner. The mobile ion and the electrolyte material distinguish them from one another. The components of a fuel cell include an anode, an electrolyte, a cathode, and possibly interlayers. The purpose of the electrolyte in a solid oxide fuel cell is to transport oxygen ions in the form of O^{2-} from the cathode to the anode, driven by an oxygen gradient between the two electrodes. To enable the oxygen ion migration across the electrolyte, oxygen reduction occurs at the cathode, converting O_2 into O^{2-}. At the anode, a fuel, such as hydrogen, accepts the O^{2-} ions and reacts to produce water and electrons. The electrons required for the reaction at the cathode are released at the anode, as the hydrogen is oxidized to H^+ ions. These electrons are conducted through an external load to the cathode, thereby producing work in the form of electricity.

The driving force behind fuel cells is the chemical gradient between the two electrodes. A high partial pressure of oxygen exists at the cathode and, conversely, at the

anode there is a low partial pressure of oxygen. Thus, a requirement of an operational fuel cell is the effective transport of oxygen ions across the electrolyte in the form of O^{2-} and not molecular O_2.

2.2 Fuel Cell Types

Three major paths exist to overcome slow reaction rates within fuel cells: the use of a catalyst, a higher operating temperature, and increasing the electrode's surface area.[4] Multiple fuel cell types exist to address the ways to overcome the slow reaction rates, as well as address the lack of hydrogen as a readily available fuel. These fuel cells are categorized by their electrolyte, such as polymer exchange membrane fuel cells which have an electrolyte consisting of a solid polymer matrix. A list of the different types of fuel cells is given in Table 1.

Type	Efficiency	Operating Temperature
Solid Oxide	45-65%	800 °C
Molten Carbonate	50%	650 °C
Phosphoric Acid	40%	200 °C
Alkaline	50-60%	80 °C
Direct Methanol	40%	80 °C
Proton Exchange Membrane	40%	50 °C

Table 1: Fuel cell types[5]

Polymer exchange membrane fuel cells (PEMFCs) have been a focus of the Department of Energy for transportation applications. This interest is partly due to their relatively low operating temperatures, ranging from 60 to 80 °C, which imparts a faster start-up time. Since these fuel cells operate at lower temperatures, the activation energy requirement is addressed by using high performance catalysts, such as platinum.

Platinum is an excellent catalyst for fuel cells and is often considered a standard to compare newly developed catalysts with. The disadvantage of platinum for PEMFCs is its scarcity and prohibitive expense.

Solid oxide fuel cells (SOFCs) are comprised of ceramic materials requiring relatively high operating temperatures, approximately 700-1000°C. Their higher operating temperature, compared to other fuel cells, affords them multiple advantages. Electrochemical reactions proceed more rapidly at higher temperature and incur less activation voltage losses. Thus, expensive noble metal catalysts may not be required. The higher operating temperature of the fuel cell and the exiting water vapor stream presents available heat to be used in a steam reformer to extract additional energy. Also, at high enough temperatures, less expensive and more readily available hydrocarbon fuels such as methane can be used and internally reformed into hydrogen for the solid oxide fuel cell to use. However, their higher operating temperature requires a longer start-up time compared to other fuel cell types and additional expense is required to heat the fuel cell power generation system. Solid oxide fuel cells have all solid-state components, such as ceramics or metals, thereby eliminating electrolyte management problems associated with such fuel cells as molten carbonate fuel cells, which have a liquid carbonate matrix electrolyte.

2.3 Applications

Fuel cell technology has not widely been exploited for commercial electricity generation, except in the past few decades. Previously, other forms of power generation have overshadowed the utilization of fuel cells, such as the combustion engine in automobiles or fossil fuel power plants for commercial electricity. With the advent of

recent environmental concerns over global warming, "cleaner" energy sources have come to the forefront of exploration and use. Fuel cell technology is one of these "cleaner" modes of electricity generation as it produces electricity with water as the sole by-product, instead of carbon monoxide, carbon dioxide, nitrogen oxides, and other pollutants from combustion engines. Also, with no moving parts like other power generation technologies, fuel cells possess improved reliability. These advantages have driven interest in fuel cell technology for a wide range of uses.

Historically, fuel cells have been a part of many important space exploration endeavors. The Apollo spacecraft program used alkaline fuel cells, not only to produce electricity for their on-board computer systems, but also to produce drinking water. They were chosen due to their higher power density output than batteries and the absence of waste by-products other than potable water. The Gemini spacecraft program used polymer electrolyte membrane fuel cells for the same reasons.

Fuel cells have more recently been used in vehicular power generation systems. In 2001, the Chrysler Natrium used an on-board hydrogen processor to produce fuel for its fuel cells and had a range of 300 miles before needing to be refueled. In 2008, Boeing developed an experimental airplane that used PEMFCs combined with lithium-ion batteries for propulsion. Fuel cells have also been employed in submarines as a way to remain submerged for weeks at a time without the need to resurface.

2.4 Advantages and Disadvantages

In addition to the formation of water as the sole by-product, fuel cells offer other advantages over other forms of electricity generation. Fuel cells have a higher theoretical and practical efficiency than combustion engines, since it is not limited by the Carnot efficiency limit which is dependent on the temperatures of input and output streams. Also, with no moving parts, fuel cells operate silently.

Fuel cell types which operate at higher temperatures such as 1000 °C have the added advantage of providing excess heat to be utilized in a steam reformer to increase overall system efficiency. This is called a combined heat and power (CHP) system and the total energy efficiency of CHP systems can range from 85-90%.[4] At these temperatures, the fuel cells can internally reform lighter hydrocarbon fuels, such as methane, eliminating the cost for additional hydrogen reformation.

However, fuel cell technology faces a number of challenges before widespread use can be adopted. The production and transport of hydrogen is challenging due to safety concerns and the fact that a hydrogen infrastructure has not been created yet. Since some fuel cells require a relatively high temperature to operate, start up times may be longer than other electricity generation technologies. Also, fuel cells may use materials such as platinum as a catalyst making them more expensive than comparable power systems.

2.5 Fuel Cell Performance

Ohmic losses between the components comprise a significant portion of the overall fuel cell's voltage loss. Even though higher operating temperatures reduce

polarization at the cathode, the cathode can contribute approximately 50% of the overall ohmic losses of the entire fuel cell.[1] The cathodic ohmic loss occurs due to the longer conduction pathways within the cathode for the electrons to travel, even though the cathode material has lower resistivity than other fuel cell components. Therefore, cathode material selection and design is a critical area of fuel cell research.

For SOFCs, one way to reduce ohmic losses is increasing the operating temperature to increase the conductivity of the perovskite materials. However, the operating temperature of the SOFCs is restricted by the fuel cell application. High operating temperatures are beneficial for power generation systems that couple SOFCs and steam reformers that utilize the high temperature water vapor exiting the SOFC. However, lower operating temperatures provide lower costs through less expensive construction methods and materials. Lower operating temperatures reduce the difference in thermal expansion coefficients between fuel cell layers, thus diminishing the effects of thermal cycling causing cracks or delamination between components, thereby destroying the fuel cell.

SOFCs operating at lower temperatures are termed ITSOFCs, or intermediate temperature solid oxide fuel cells. ITSOFCs offer the advantage of lower cost materials, reduced degradation due to thermal cycling and operation, as well as shorter start-up times to achieve the required operating temperature. However, higher ohmic losses are incurred by operating at these lower temperatures due to an increased resistivity of the materials.[1] Material selection and design is therefore another area of research with the goal of fabricating less expensive and higher performing ITSOFCs.

2.6 The Triple Phase Boundary

At the anode surface, hydrogen reacts, thereby releasing energy. However, this reaction proceeds at the classical energy model for a simple exothermic reaction. The activation energy must be overcome to release energy. If the probability of the molecule having the required activation energy is low, the reaction proceeds slowly and little energy is released. Three main paths to overcome a slow reaction rate are: the use of a catalyst, a higher operating temperature, and increasing the electrode's surface area.[4]

The site where the gases are simultaneously in contact with the electrolyte as well as the cathode is called the triple phase boundary. Increasing the triple phase boundary, for instance through the use of mixed ionic and electronic conducting electrode materials, effectively increases the electrode's active surface area where the reduction/oxidation reactions occur. Fabricating a highly porous electrode microstructure is another way to increase the surface area, creating more catalytically active reaction sites and resulting in more energy released.

2.7 Nernst Equation

Work is performed by the fuel cell by transporting electrons across a voltage difference, from one potential to the other. The work done by the fuel cell is the product of the electric potential difference and the charge transported. If the charge transport is performed reversibly, the electric potential difference between the two electrodes is called the electromotive force, E.[6]

As mentioned previously, the driving force for fuel cells is the difference between chemical potentials of oxygen at the electrodes. This is expressed as the Nernst equation,

shown in Fig. 1, using the general fuel cell reaction utilizing pure hydrogen and oxygen, where E is the reversible cell voltage, R is the gas constant, T is temperature, F is Faraday's constant, and $P_{(O2)}$ is the partial pressure of oxygen at the anode/cathode.

$$E = \frac{RT}{4F} \ln \frac{P_{O_{2(c)}}}{P_{O_{2(a)}}}$$

Fig. 1: Nernst equation

2.8 Solid Oxide Fuel Cell: Anode

The purpose of the solid oxide fuel cell anode is oxidizing the hydrogen fuel with oxygen ions conducted through the electrolyte from the cathode. The anode of the fuel cell is a cermet, a mixture of solid ceramic material and a metal catalyst. Yttria-stabilized zirconia is commonly used as the ceramic component for SOFC anodes and its addition into the anode structure, along with the metal catalyst, functions to provide a thermal expansion coefficient similar to that of the electrolyte, which will be discussed in further detail below. The anode is designed to have a sufficient porosity, approximately 20-40%, to enhance transport of the reactant and product molecules.[7]

The metal catalyst within the anode most commonly is nickel, which is combined with a ceramic component. Nickel is stable under reducing conditions, it possesses a high electronic conductivity at high temperatures, and it is a relatively inexpensive catalyst. Within the reducing hydrogen environment, the nickel oxide is reduced to elemental nickel, creating a nickel surface on the anode's pores. The hydrogen is chemisorbed onto the nickel surface and hydrogen ions react with oxygen ions at the

electrolyte surface. The liberated electrons are then transferred, via a current collector, to an external circuit.

Hydrocarbon fuels will form coke (carbon) deposits on the nickel catalyst surface and sulfur impurities that are present in hydrocarbon fuels poison the anode by reacting with the nickel atoms to form nickel sulfide. Therefore, one current area of research is finding a mixed ionic/electronic conductor which has the following features: chemical stability in the reducing anode atmosphere, similar thermal expansion with surrounding fuel cell layers for compatibility, high electronic conductivity, oxide-ion conductivity, minimal electrical resistance, and fast dissociation of the chemisorbed fuel.[4] Oxygen-deficient double perovskites such as strontium magnesium molybdenum oxide, or SMMO, are one such material with the possibility to meet all of these criteria.[8]

Anode material selection is an area of research to add desired qualities, such as improved sulfur tolerance, to the fuel cell. Lanthanum strontium gallium manganese oxide (LSGM) is one such sulfur tolerant anode that is a promising anode material for intermediate temperature solid oxide fuel cells.[9] The addition of small amounts of cerium (IV) oxide has been shown to improve the resilience of the anode against temperature cycling and repeated transitions between a reducing environment and a non-reducing environment.[4] Alternate anode materials, such as titanium dioxide, TiO_2, are also being studied to focus on the direct utilization of methane instead of first reforming the hydrocarbon fuel into pure hydrogen.

2.9 Solid Oxide Fuel Cell: Electrolyte

The electrolyte of the solid oxide fuel cell is required to be an oxygen ion conductor while being electrically insulating to prevent short-circuiting the fuel cell. The electrolyte material has not changed significantly since 1899, when Nernst discovered zirconia, ZrO_2, as being a sufficiently good conductor of oxygen above 800 ^{o}C. Since then, 8-10 mole % of yttria, Y_2O_3, has been used to dope the zirconia ceramic to improve its ionic conductivity, forming the ubiquitous electrolyte material for SOFCs used today, yttria-stabilized zirconia, YSZ.

The increased ability of YSZ to conduct oxygen ions comes from vacant oxygen sites formed within the microstructure. Zirconia has a fluorite crystal structure containing Zr^{4+} ions. When 8-10 mole % yttria is added, some of the Zr^{4+} ions are replaced with Y^{3+} ions in the crystal structure. The Kroger-Vink notation of this event is shown in Fig. 2. One oxygen vacancy (V_o) is formed for every mole of Y_2O_3 dopant. Vacant oxide-ion sites within the perovskite lattice allow oxide-ion flow to occur at these sites. The ionic conductivity of YSZ can be 0.02 S/cm at 800 ^{o}C, making its ionic conductivity comparable to electrolyte materials used in other fuel cell types, such as the liquid carbonate matrices used in MCFC's.[10] The YSZ electrolyte is made as thin as possible to lower the internal resistance of the fuel cell.

$$Y_2O_3 \rightarrow 2Y'_{Z_r} + 3O_o + \frac{1}{2}V_o$$
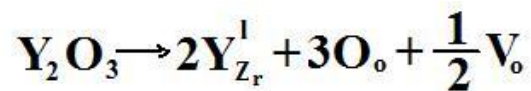
Fig. 2: Kroger-Vink notation for the doping of Zr with Y_2O_3

The YSZ electrolyte is a very effective material for multiple reasons. First, it is very stable at high temperatures in both reducing environments and oxidizing ones, which is the reason it can be used as the electrolyte and the ceramic anode component. This allows for a more congruent thermal expansion coefficient between the two layers, providing overall fuel cell stability during high temperature operation, thermal cycling, and sintering processing steps.

Alternate electrolyte materials have been investigated which have increased oxygen-ion conductivity at lower operating temperatures than YSZ, 0.02 S/cm at 800°C.[10] One such material is lanthanum strontium gallium manganite, LSGM, which can reach an oxygen-ion conductivity of 0.02 S/cm at 650 $^{\circ}$C. Although other materials exist, such as BiVCuO or CeGdO, which have better oxygen ion conduction capabilities than YSZ or even LSGM, they also must be sufficiently stable at the low oxygen partial pressures found at the SOFC anode layer, making alternative electrolyte material selection challenging.

2.10 Solid Oxide Fuel Cell: Cathode

Many cathode materials used in SOFCs today, such as LSM, are p-type semiconducting perovskite structures.[11] P-type semiconductors are created by the use of dopants to increase the number of free positive charge carriers. The dopant accepts weakly bound valence electrons from the semiconductor, leaving an electron vacancy. These vacancies are used as positive charge carriers within the cathode. This property is opposite of an n-type semiconducting material where the dopant atoms provide additional electrons to the host material, creating an excess of negative charge carriers.

The purpose of the cathode is to transfer electrons from the external circuit to adsorbed oxygen molecules, reducing oxygen to its negatively charged oxygen ion components, and to then transfer them to the electrolyte layer. The oxygen molecule chemisorbs onto an oxide-ion vacancy of the cathode material. The cation must have an electron of sufficiently high energy to donate electrons to the antibonding orbitals of the oxygen molecule, thereby breaking the double bond holding the oxygen molecule together.

An optimum cathode choice will be one that is able to rapidly catalyze the reduction of oxygen and is chemically stable in the oxidizing environment. Oxygen is mobile on an oxide's surface so the material need not be ion conducting to operate, however, this mixed ionic/electronic conduction capability would afford the utilization of the bulk material, instead of just cathode particle surface area, creating more catalyst reaction sites, thereby improving overall fuel cell performance. Mixed ionic/electronic conduction cathodes are generally perovskites of the form ABO_3.[1] The A-site is usually lanthanum doped with an alkaline earth metal, such as strontium or calcium. The B-site is a transition metal such as chromium, manganese, iron, cobalt, or nickel. These perovskite materials are chemically stable, chemically compatible with the electrolyte, and have a thermal expansion coefficient similar to that of the electrolyte which is usually YSZ.

The cathode of the fuel cell was originally made from expensive noble metal catalysts such as platinum; however, less expensive ceramics are currently employed. The two types of cathodes are those that are solely electronically conductive oxides and

ones that have mixed electronic and ionic conduction capabilities. Lanthanum strontium manganite, or LSM, is a common electronic conductor cathode material.

Lanthanum strontium manganite is a perovskite with a thermal expansion coefficient compatible with that of YSZ. It does not have sufficient ionic conduction capabilities since the mixed-valent Mn^{4+}/Mn^{3+} redox energy is prohibitively high to retain enough oxygen ion vacancies in an oxidation environment at the high operating temperatures of the fuel cell. However, the surface provides reaction sites with electrons of high enough energy to convert oxygen molecules into peroxide ions, O_2^{2-}. One oxygen atom within the peroxide ion travels to another reaction site on the surface of the cathode material to create two O^{2-} ions. These oxygen ions travel to the triple phase boundary on the cathode side to be shuttled through the electrolyte. The reaction site locations, being only at the surface of the cathode material, require a highly porous cathode material to provide sufficient catalytic activity.[2]

Mixed ionic and electronic conducting cathode materials not only possess reaction sites at the surface, but within the bulk material as well. These materials must replenish oxygen vacancies at the reaction sites as rapidly as oxide ions leave the anode surface. Lanthanum strontium cobalt ferrite, LSCF, has been found to have improved mixed conduction properties over LSM. This approach increases the effective area of the triple phase boundary region and thereby improves the overall electrochemical performance of the fuel cell. LSCF has a total conductivity of 230 S/cm at 900 ^{o}C, similar to that of LSM, however it also has an oxygen ionic conductivity of 0.2 S/cm.[12] In contrast, LSM has an oxygen ionic conductivity of only 10^{-7} S/cm making it a very poor ionic conductor. Mixed ionic and electronic conductivity is important since the polarization of

the cathode increases at lower temperatures. At 650 ^{o}C and below, the advantages of using a material with such a mixed conductivity become more apparent.

2.11 Fabrication Techniques

A very common technique for fuel cell fabrication is tape casting. In this method a slurry of suspended ceramic material is spread over a flat surface, creating a length of tape. The height of the doctor blade and the properties of the slurry affect the thickness of the tape, thereby determining the thickness of the fuel cell layer. The tape must be sintered at high temperatures to form the stable solid structure used in the fuel cell. The disadvantages involved with sintering at high temperatures include undesirable reactions occurring between different components of the fuel cell and increased coarsening of the catalyst microstructure, leading to reduced catalytically active surface area.

Data driven direct-write methods, DDDW, are another class of fuel cell fabrication and these methods have been explored for solid oxide fuel cell fabrication using LSM as the cathode. These DDDW methods include ink jet deposition and, more recently, aerosol jet deposition. Both techniques employ a computer controlled nozzle to deposit the desired material onto a substrate to form a fuel cell in subsequent layers.

In the aerosol jet deposition technique, an ink comprised of a carrier solvent, the material to be deposited, pore formers, binders, and plasticizers, is placed into a reservoir. Then, the ink is atomized into droplets suspended in a carrier gas such as dry air or high purity nitrogen to create an aerosol. The aerosol travels into a deposition head and is deposited onto a substrate. The location of the deposition head in relation to the substrate is computer-controlled by a motorized platen. Intricate patterns of deposited material can

be formed, affording precise control over the fuel cell's formation in all three dimensions without contacting the substrate material, allowing for deposition onto planar or curved substrates. The computer controlled fabrication system allows for highly reproducible SOFC fabrication compared to other methods. The AJDT had been used in the formation of solar cells but only recently has it been used to fabricate fuel cells.

3. Experimental

3.1 Aerosol Jet Deposition Technique: Inks

Inks are used within the Aerosol Jet Deposition Technique as a carrier for the desired ceramic material comprising the fuel cell layer being deposited. Inks were devised and created based on strategies and recipes found in the literature and then the recipes were modified to be used to print solid oxide fuel cells using the Optomec Aerosol Deposition system.   This system can be seen in Fig. 3.
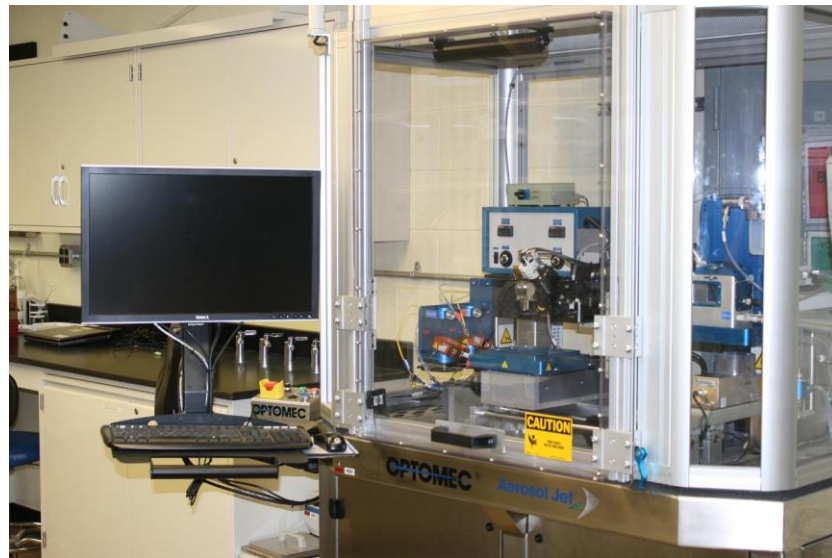
Fig. 3: Optomec Aerosol Deposition System

These inks used 8 mol% yttria stabilized zirconia (8YS, Tosoh Corporation), gadolinium doped cerium oxide (GDC10-HP, NexTech Materials), and lanthanum strontium cobalt ferrite (99.9% $La_{0.6}Sr_{0.4}Fe_{0.8}Co_{0.2}$ Oxide, Praxair Surface Technologies) as the ceramic materials.   Solvents used in the inks were 2-butanol (99%, Alfa Aesar) and α-terpineol (96%, Alfa Aesar).   These were chosen for their higher boiling points

than other alcohol solvents, equating to a slower drying rate. The ratio of 2-butanol to α-terpineol was chosen at 5.67:1 for the inks. The dispersant used in the inks was Disperbyk-111 (BYK USA Inc.), a phosphate polyester, to keep particles in suspension. Binders and plasticizers used were ethyl cellulose (Y), polyalkylene glycol (Richard E. Mistler, Inc.), butyl benzyl phthalate (Richard E. Mistler, Inc.), and polyvinyl butyral (Richard E. Mistler, Inc.). Binders promote adhesion of the ceramic suspension to the substrate after evaporation of the solvent, discouraging the formation of defects and cracks. Ink components were added together in a glass wheaton bottle and 5 mm diameter ceramic zirconia beads were used in conjunction with a ball mill to mix the ink overnight. The amount of ceramic material was tailored specifically for each type of ink and experiment.

A high particle loading of the ink can decrease the porosity of the resulting sintered microstructure. Also, the higher the particle loading, the more viscous the ink will be and the less likely it will be able to atomize sufficiently for the aerosol jet deposition technique to be used. Inks were characterized using an Anton Paar Rheolab QC to measure viscosity. Viscosity also plays an impact on ink stability as suggested by Stokes' Law which can approximate the amount of settling of a particle over time, shown in Fig. 4. Here, R is the radius of the ceramic particles, g is the acceleration due to gravity, v_s is the settling velocity, p_p and p_f are the densities of the particle and the fluid, and μ is the viscosity of the fluid. We can see mathematically that the viscosity of the fluid has an inverse relationship with settling velocity, thus higher viscosity inks will suspend particles for a longer duration. Ink stability is not directly influential on fuel cell performance but will affect the deposition technique used to fabricate the fuel cell.

$$v_s = \frac{2}{9}\frac{\left(\rho_p - \rho_f\right)}{\mu}g\,R^2$$

Fig. 4: Stoke's law for gravitational settling

3.2   Anode Support Substrates

Composite anode material sheets consisting of 55% yttria stabilized zirconia and 45% nickel oxide were used as the solid oxide fuel cell support upon which subsequent electrolyte, buffer, and cathode layers were deposited using the aerosol jet deposition technique. The composite anode material sheets were cut using a punch to produce circular wafers which would become the solid oxide fuel cell supports. The composite anode material wafers were then bisque-fired in a furnace at 950°C to impart mechanical stability and a favorable porous anode microstructure for increased hydrogen gas diffusion. The substrates had an approximate thickness of 800 microns following bisque-firing. A bisque-fired substrate can be seen in Fig. 5.

Fig. 5: Bisque-fired anode substrate

3.3   Aerosol Jet Deposition Technique

Inks were deposited onto the substrate using the Optomec system, which utilized the aerosol jet deposition technique to produce each layer of the solid oxide fuel cell in sequence, aside from the composite anode substrate support. To ensure consistent results, inks were prepared within 48 hours of deposition. A prepared LSCF ink can be seen in Fig. 6.

Fig. 6: Prepared LSCF ink within a wheaton bottle container

The Optomec system has three-dimensional control of how the aerosol jet is laid onto the surface of the substrate. The AutoCAD pattern determines the x and y positioning of the fuel cell substrate while the Optomec system's nozzle, through which the aerosol jet leaves, is depositing onto the fuel cell substrate. A nozzle designed for a wide aerosol deposition was used which has a 2.5 mm x 0.5 mm oval-shaped orifice. The deposition nozzle head can be seen in Fig. 7. By altering the z-height of the nozzle, the aerosol jet is closer or farther away from the substrate. Farther away, the nozzle produces a very fine and scattered aerosol deposition, which translates to a more porous fuel cell layer. If the z-height of the nozzle is very close, the aerosol jet produces a denser layer.
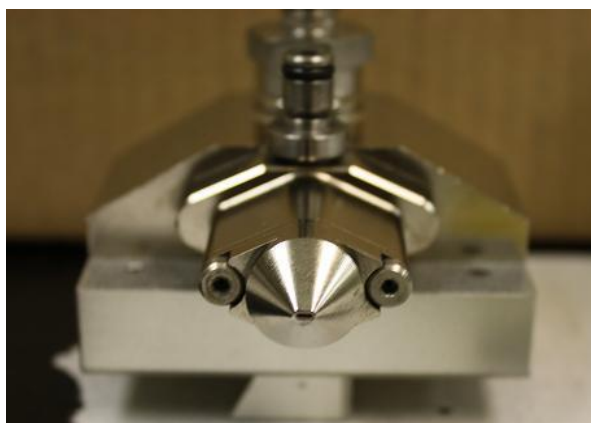
Fig. 7: Deposition nozzle head of the Optomec AJDT system

Using AutoCAD 2009 software and VMtools, a computer program was written that the Optomec system would recognize and follow to create a deposition pattern of the different fuel cell layers. This alternative to masking or lithography techniques produces the desired pattern onto the fuel cell. The pattern created for this experiment blankets the fuel cell with the proper ink to create a homogeneous fuel cell component layer. The Optomec system's nozzle passes back and forth in a raster pattern. The spacing between each pass of the nozzle is called the "y-spacing" since it is the Optomec system's control in the y-direction. If this y-spacing is farther apart, a more porous fuel cell layer is deposited. Conversely, if the y-spacing is close together, a denser layer results.

A variety of parameter settings were chosen to successfully deposit ink onto the substrates, as shown in the Results section. Desiccant-dried laboratory air was used as the carrier gas for inks. Pure nitrogen gas is one alternative carrier gas for the AJDT system. Three flow rates were set to deposit ink onto the fuel cell surface. The sheath flow rate was used to direct the aerosol stream onto the substrate surface. A higher sheath pressure produces a narrower aerosol jet and a lower sheath pressure will produce

a wider aerosol jet. A wider aerosol jet is thought to increase porosity of the sintered material. The vacuum flow rate removes a certain amount of aerosolized particles which is being atomized. This flow rate influences the size distribution of the aerosol droplets being deposited onto the fuel cell. The atomizer pressure dictates the amount of ink that eventually deposits in aerosol form onto the fuel cell substrate surface. A higher atomizer pressure produces more deposition and a lower atomizer pressure will produce little to no deposition. The atomizing pressure provides a feedback mechanism for monitoring the status of the aerosol jet nozzle. The atomizer can be seen in Fig. 8.

Fig. 8: Atomizer within the Optomec AJDT system

Only one fuel cell layer used a masking technique. A masking of Kapton tape was placed over the fuel cells before the LSCF cathode material was deposited. The mask covered the fuel cell except for a circle of diameter 0.5 in. (or 1.3 cm). From the dimensions of the resulting cathode layer that was deposited, it was determined that the active surface area for the fuel cells is 0.196 in^2 (or 1.26 cm^2). A set of finished fuel cells with the LSCF cathode and CGO buffer layers visible is seen in Fig. 9. The masking effect can clearly be seen.

Fig. 9: A set of four completed fuel cells with the black LSCF layer visible on top

3.4 Deposition and Sintering Profiles

The composite anode substrate supports to be printed on were placed into the Optomec system and the YSZ ink was loaded. The computer program containing the printing pattern for the electrolyte layer was loaded to be used. Following the deposition of YSZ ink onto the substrate, the fuel cells were dried on a heat platen set to 60°C to partially dry the solvents. The fuel cells were then removed and placed onto a tray, ready to be sintered.

The fuel cells were placed into a programmable furnace and a sintering profile program was created, the details of which are described in Section 3.12. The purpose of sintering the fuel cell is to impart mechanical stability and to produce a favorable porous or dense microstructure once the pore formers and solvents have evaporated. The fuel cells rested on an alumina plate to reduce diffusion of materials into or out of the cells during heat treatment. A second alumina plate was rested on top of the cells to promote a

flat and even fuel cell. These cells were then placed between two ceramic trays in the furnace to provide more uniform and distributed heat conduction to the fuel cells.

This process was repeated using the different inks, the only difference being a weight was not applied on top of the fuel cells after the buffer or cathode layers were printed. Each material had a unique sintering profile. The order they were printed onto the anode substrate was: electrolyte, CGO buffer layer, and then LSCF cathode layer. After the cells were sintered for the last time, they were ready for electrochemical testing or characterization.

3.5 Electrochemical Testing

Before testing the fuel cells in a high temperature environment, they must have conductive leads attached to their anode and cathode sides and they must be mounted onto an apparatus for fuel delivery for the anode. Approximately two pieces, six inches each, of silver wire (99.9985% Premion, 0.5 mm diameter) were manipulated into an M-shape configuration. One piece of silver wire was placed over the anode and gold conducting paste (C5729 Gold Conductor Paste, Heraeus) was used to secure it to the surface of the anode. A small amount of high temperature paste (Ultratemp 516, Aremco Products) was put onto the silver wire (away from the active surface area of the fuel cell) to help secure it to the fuel cell. The fuel cell was then placed into an oven at 90°C for 10 minutes, then 150°C for 10 minutes, followed by cooling to room temperature. A second piece of silver wire was placed over the cathode and gold conducting paste was used to secure it to the cathode. A small amount of high temperature paste was used as before. The fuel cell was then placed into an oven at the same temperature profile as described above. The fuel cells with test leads attached can be seen in Fig. 10.

Fig. 10: Fuel cells with silver wire test leads in M-shape configuration

The fuel cell was mounted onto a hollow alumina tube. The hollow alumina tube has an outer diameter of 1 in. and inner diameter of 0.8 in. High temperature paste was applied to the edge of one side of the tube and the anode side of the fuel cell was placed face down onto it. Then, high temperature paste was placed around the edge of the fuel cell to secure it and to make it air-tight. A small weight was placed over the fuel cell to secure it in place and the high temperature paste was allowed to cure at room temperature for approximately 2 hours. A device used to provide fuel delivery to the anode side of the fuel cell was inserted into the hollow alumina tube. The four ends of silver wire were connected to the Solartron for polarization experiments.

The fuel cell apparatus was placed into a programmable furnace for testing. A flow controller was used to correctly administer chosen amounts of gases to each side of the fuel cell. A flow of 5% hydrogen and 95% argon gas was provided at 32 cc/min while the furnace was set to 650 °C to reduce the fuel cell. The nickel oxide is reduced to nickel in the hydrogen environment. The fuel cell was allowed to remain in this reducing environment for approximately 15 hours. Then, the gas was switched to 100 % hydrogen

for 1.5 hours with a flow rate of 48 cc/min while the furnace was set to 650°C at which point the fuel cell was ready to be tested.

A Solartron instrument (1470E and 1400 Cell Test Systems, Solartron Analytical) was used to provide impedance plots and polarization curves for the fuel cell being tested. A flow rate of 48 cc/min of 100% hydrogen was used to provide fuel to the anode. The test electrodes of the Solartron instrument were attached to the four silver wire ends attached to the fuel cell.

The CellTest computer program was used to provide settings for and record data from the Solartron. The program first rested for 60 seconds. Then, it performed an impedance sweep from 1 MHz to 50 mHz in 10 steps per decade. For the impedance sweep, an AC voltage of 10 mV was applied. Next, the program rested for 60 seconds again. Then, it performed a polarization curve by ramping from OCV, or open circuit voltage, to -940 mV of the open circuit voltage over 200 seconds. This polarization curve was voltage controlled, not current controlled. These measurements were executed at each temperature tested: 650°C, 700°C, 750°C, and 800°C. Once all measurements were complete, the furnace was set to room temperature and then the fuel cell was removed after cooling.

3.6   Scanning Electron Microscopy Characterization

The scanning electron microscope (SEM) used was a JSM-6060 model with energy-dispersive x-ray spectroscopy (EDAX) capabilities. The EDAX system was Noran System SIX. The SEM images were used to determine various microstructure parameters such as grain size and thickness of each layer. The fuel cells were prepared

for SEM imaging before placing them into the specimen chamber. The specimen chamber of the JSM-6060 can accommodate 5 in. diameter specimens. Each fuel cell was broken into pieces and mounted onto an angled steel stand with carbon tape. The broken edge of the fuel cell was faced outwards from the stand. This allowed a top-down image to be taken of the fuel cell surface and a cross-section image to be taken of the broken edge.

After the sample was prepared, the sample was loaded into an airlock chamber connected to the sample chamber. Next, the airlock chamber had its pressure decreased to match the vacuum environment of the sample chamber. The airlock and sample chambers were then opened to each other and the fuel cell sample was placed in front of the electron beam.

The settings for the SEM were then set. The AC voltage was 10 kV for each sample. The working distance used for the SEM images was 10 mm. Magnifications for top-down and cross-section images were: 500x, 1000x, 5000x, and 10000x. Afterward, the SEM images were analyzed using the ImageJ software which used calibrated markings to measure grain size and layer thickness.

3.7   Viscosity Measurements

Viscosity is an important characteristic of the inks to determine printability with the AJDT system and also to determine the shelf life of the ink. A less viscous ink would be more likely to atomize sufficiently but a more viscous ink would possess a longer shelf life. The viscosities of the inks were measured using an AntonPaar Rheoplus. The ink to be tested was loaded into the 20 mL chamber. A spinning steel tip measured the

viscosity in mPa•s at different shear rates. Thirty viscosity measurements were taken over shear rates ranging from 0 to 1300 1/s.

3.8   Hydrodynamic Diameter

Dynamic light scattering (DLS) was performed on a variety of inks to measure the hydrodynamic diameter of the particles within the inks. The instrument used was a Malvern Instruments Zetasizer Nano-ZS. The hydrodynamic diameter is the effective diameter of suspended particles. DLS measures the diffusion of particles moving under Brownian motion, then calculates a size distribution using the Stokes-Einstein equation. Different ethyl cellulose chain lengths should coat the particles and alter the hydrodynamic diameter.

A set of four inks was formulated with varying ethyl cellulose types.   A table of the ink recipes is shown in Table 2. The ethyl cellulose types included: ethyl cellulose 45, ethyl cellulose 200, ethyl cellulose 300, and ethyl cellulose (Y). One limitation, imposed by the instrument, on the inks was fewer than 50 µg of particles per mL could be utilized, which required diluting the ink samples to 4 mg LSCF per ink. Next, 750 µL of sample was placed into the Folded Capillary Cell sample holder using a pipette, ensuring no air bubbles entered the sample holder. Then, the sample holder was placed inside the cuvette chamber and the refractive indices of the solvents were entered into Malvern's Dispersion Technology Software.

Amount	Components
23	g 2-butanol
4	g a-terpineol
0.09	ethyl cellulose type
	stir at 100C with lid on
4	mg LSCF
0.24	g D111
	3 hours on ball mill
0.18	g PAG/BBP/PVB
	ball mill overnight

Table 2: Ink formulations for DLS measurements

3.9   Gel Permeation Chromatography

Different types of ethyl cellulose ink additives were analyzed using gel permeation chromatography (GPC). This GPC uses size exclusion to separate the analyte based on the polymer's size. The specific instrument was a Viscotek Model 270 dual detector. The ethyl cellulose samples were differing types obtained from Dow Chemical: EC 45 industrial grade, EC 200 industrial grade, EC 300 industrial grade, and then EC (Y) was from an unidentified source. The ethyl cellulose samples were dried in a desiccator prior to GPC analysis to enhance detection. A triple calibration was performed to incorporate all four detectors including refractive index, DP viscometer, low angle light scattering (LALS), and right angle light scattering (RALS). Only refractive index and DP measurements were reported. The results showed the molecular weights and the polydispersity indices of each ethyl cellulose type. The polydispersity index of a polymer is a measure of the distribution of molecular mass.

3.10   Relationship Between Number of Passes and Thickness

The buffer and electrolyte layers were designed to be thin, to reduce resistance, but dense enough not to allow gas diffusion to occur between the two electrodes. The buffer layer was desired to be dense and approximately 5 microns thick after sintering so an experiment was devised to determine the number of passes required with the AJDT to produce this thickness with CGO. The LSCF cathode layer's thickness after sintering was found in the same manner. The ink recipes used to determine the relationship between thickness and the number of passes can be seen in Table 3.

CGO Ink Recipe	LSCF Ink Recipe	Components
9.5	0	g CGO
0	24.5	g LSCF
29.75	38.25	g 2-butanol
5.25	6.75	g terpineol
0.18	0.15	g EC(Y)
0.31	0.4	g D111
shake	shake	
0.23	0.3	g PAG/BBP/PVB
ball mill	ball mill	

Table 3: CGO and LSCF ink recipes

First, two anode substrates were printed using the AJDT with a CGO layer. Next, the two fuel cells were sintered at 1250 ^{o}C for 2 hours. Then, an LSCF layer was printed and then the fuel cells were sintered again at 1080 ^{o}C for 2 hours. The AJDT parameters were set to nominal values used in subsequent experimentation with the assumption that the number of passes would be directly proportional to the thickness if all other AJDT parameters were equal. A summary of the AJDT parameters used to determine the relationship between the number of passes and the thickness of sintered CGO and LSCF

layers can be seen in Table 4. Alterations to the AJDT parameters may influence the

resulting thickness.

AJDT Parameters	Parameter
Raster	Program
Dehydrated Air	Carrier gas
3000	Sheath Pressure (sccm)
1350	Vacuum Pressure (sccm)
1500	Atomizer Pressure (sccm)
-24	z-height
100	Print speed (mm/sec)
0.17	y-spacing (mm)
24	# of passes

Table 4: AJDT Parameters used to determine thickness per the number of passes

The cells were broken into pieces and SEM images were taken of their cross-

sections. ImageJ software was used to determine the average thickness of the CGO and

LSCF layers after sintering. By knowing the distances between calibration points on the

SEM image, the average thickness of the CGO and LSCF layers could be determined.

3.11 Preliminary Fuel Cell Fabrication Study and Baseline Experiment

A preliminary study was needed to determine a baseline set of fuel cell fabrication

parameters before a fuel cell with the newly used LSCF could even be printed. This

baseline set selection involved manipulating multiple AJDT parameters, such as layer

thickness and y-spacing, performing a series of measurements on the fuel cells created,

and then selecting one set of AJDT parameters as the standard to use for the other two

experiments. One difficulty of altering AJDT parameters is due to their interdependency,

meaning a change in one parameter will result in a required change in another parameter.

One purpose of this preliminary study was to be able to successfully deposit the LSCF ink using the AJDT technique onto a substrate and to manipulate the microstructure to ascertain how far the LSCF microstructure could be altered using the AJDT technique.

Three sets of identical pairs of fuel cells were fabricated using different combinations of AJDT variables to test their contribution to the cathode microstructure and to determine a baseline set of AJDT parameters to be used. The first identical pair of fuel cells was created with the ink recipes and AJDT parameters shown in Table 5 and Table 6, respectively. These settings were chosen to produce a denser microstructure, utilizing a shorter y-spacing and shorter z-height to the substrate. First, two anode substrates were printed on using the AJDT with a CGO layer. The two fuel cells were then sintered at 1250 ^{o}C for 2 hours. Then, an LSCF layer was deposited and the fuel cells were sintered again at 1080 ^{o}C for 2 hours. Lastly, the fuel cells were tested using SEM, EDAX, and with polarization studies using the methods described in previous sections.

The next identical pair of fuel cells was created with the ink recipes and AJDT parameters shown in Table 5 and Table 6, respectively. These settings were chosen to produce a more porous microstructure than the previous set, utilizing a wider y-spacing and further z-height to the substrate. The same processing steps and characterization studies were performed for this pair of fuel cells as the first pair.

First pair CGO	First pair LSCF	Second pair CGO	Second pair LSCF	Components
9.5	0	0	0	g n-Gimat CGO
0	0	9.5	0	g Fuelcellmaterial CGO
0	24.5	0	24.5	g LSCF
29.75	38.25	29.75	38.25	g 2-butanol
5.25	6.75	5.25	6.75	g terpineol
0.18	0.15	0.18	0.15	g EC(Y)
0.31	0.4	0.31	0.4	g D111
				shake
0.23	0.3	0.23	0.3	g PAG/BBP/PVB
				ball mill

Table 5: Ink recipes for first two pairs of fuel cells

First pair: CGO	First pair: LSCF	Second pair: CGO	Second pair: LSCF	
AJDT Parameters	AJDT Parameters	AJDT Parameters	AJDT Parameters	Parameter
Raster	Raster	Raster	Raster	Program
Dehydrated Air	Dehydrated Air	Dehydrated Air	Dehydrated Air	Carrier gas
3000	3000	3000	3000	Sheath Pressure (sccm)
1350	1350	1350	1350	Vacuum Pressure (sccm)
1500	1500	1500	1500	Atomizer Pressure (sccm)
-23.2	-23.2	-23.2	-15	z-height
100	100	100	100	Print speed (mm/sec)
0.17	0.17	0.17	0.5	y-spacing (mm)
6	24	6	128	# of passes

Table 6: AJDT Parameters for first two pairs of fuel cells

The settings for the last identical pair were chosen to produce a microstructure in between the previous two pairs. The cathodes of the last identical pair of fuel cells were created with the ink recipes and AJDT parameters shown in Table 7 and Table 8, respectively. The CGO layer was sintered at 1250 ^{o}C for 2 hours. Then, an LSCF layer

was deposited and the fuel cells were sintered again at 1080 ^{o}C for 2 hours. The same characterization studies were performed for this pair of fuel cells, as before.

AJDT Parameters	Parameter
Raster	Program
Dehydrated Air	Carrier gas
3000	Sheath Pressure (sccm)
1350	Vacuum Pressure (sccm)
1500	Atomizer Pressure (sccm)
-23.2	z-height
100	Print speed (mm/sec)
0.25	y-spacing (mm)
60	# of passes

Table 7: AJDT Parameters for the cathode layer of the third pair of fuel cells

LSCF Recipe	Components
23	g 2-butanol
4	g a-terpineol
0.09	EC(Y)
	stir at 100C with lid on
14.7	g LSCF
0.24	g D111
	3 hours on ball mill
0.18	g PAG/BBP/PVB
	ball mill overnight

Table 8: LSCF ink recipe used for third pair of fuel cells

3.12   Experiment 1: Microstructure Change Due to Sintering

Using the established set of baseline parameters from Section 3.11, four sets of identical pairs of fuel cells were fabricated using different sintering profiles to test the sintering profiles' contribution to the cathode microstructure. One set of ink recipes and AJDT parameters were used for all 8 fuel cells. These are listed in Table 9 and Table 10,

respectively. The CGO layers were sintered at 1200 $^{\circ}$C for 2 hours, then 1250 $^{\circ}$C for 2 hours. Then, the LSCF layer was deposited and the fuel cells were sintered at varying sintering profiles, as depicted in Table 11. Next, SEM characterization was performed with ImageJ software, as described in a previous section, to determine the cathodic microstructure changes created by using the different sintering profiles.

CGO Recipe	LSCF Recipe	Components
46	23	g 2-butanol
8	4	g a-terpineol
0.18	0.09	EC(Y)
		Stir at 100°C with lid on
14.7	0	g CGO
0	14.7	g LSCF
0.48	0.24	g D111
		3 hours on ball mill
0.36	0.18	g PAG/BBP/PVB
		ball mill overnight

Table 9: Ink Recipes

AJDT Parameters	Parameter
Dehydrated Air	Carrier gas
3000	Sheath Pressure (sccm)
1350	Vacuum Pressure (sccm)
1500	Atomizer Pressure (sccm)
-23.2	z-height
100	Print speed (mm/sec)
0.25	y-spacing (mm)
60	# of passes

Table 10: AJDT Parameters for LSCF layer

Cell identifier	Step 1	Step 2	Step 3	Step 4
P5 and 6	ramp to 500 °C at 1 °C/min	ramp to 1080 °C at 3 °C/min	dwell 2 hours at 1080 °C	ramp to 0 °C at 4 °C/min
P7 and 8	ramp to 500 °C at 1 °C/min	ramp to 1020 °C at 3 °C/min	dwell 2 hours at 1020 °C	ramp to 0 °C at 4 °C/min
P9 and 10	ramp to 500 °C at 1 °C/min	ramp to 1120 °C at 3 °C/min	dwell 2 hours at 1120 °C	ramp to 0 °C at 4 °C/min
P11 and 12	ramp to 500 °C at 1 °C/min	ramp to 1050 °C at 3 °C/min	dwell 2 hours at 1050 °C	ramp to 0 °C at 4 °C/min

Table 11: Sintering temperature profiles

3.13 Experiment 2: Microstructure Change Due to Binder

Three fuel cells were fabricated using different ethyl cellulose types as an ink additive to test its contribution to the cathode microstructure. The addition of ethyl cellulose to the ink can affect the viscosity and stability of the ink and can affect the porosity of the final sintered microstructure. The different ethyl cellulose types were: ethyl cellulose 45 industrial grade, ethyl cellulose 200 industrial grade, and ethyl cellulose (Y). These were chosen to represent a range of ethyl cellulose types. The ink recipes differ only by the ethyl cellulose additive, as seen in Table 12. One set of AJDT parameters was used for the three fuel cells and are listed in Table 13. The CGO layer was sintered at 1250 $^{\circ}$C for 2 hours. Then, an LSCF layer was deposited and the fuel cells were sintered at 1080 $^{\circ}$C for 2 hours. SEM characterization was performed with ImageJ software, as described in a previous section, to determine the cathodic microstructure changes created by using the different ethyl cellulose types.

CGO Recipe	EC 45 LSCF Recipe	EC 200 LSCF Recipe	EC(Y) LSCF Recipe	Components
46	23	23	23	g 2-butanol
8	4	4	4	g a-terpineol
0	0.09	0	0	EC(45)
0	0	0.09	0	EC(200)
0.18	0	0	0.09	EC(Y)
				Stir at 100°C with lid on
14.7	0	0	0	g CGO
0	14.7	14.7	14.7	g LSCF
0.48	0.24	0.24	0.24	g D111
				3 hours on ball mill
0.36	0.18	0.18	0.18	g PAG/BBP/PVB
				ball mill overnight

Table 12: Ink Recipes

AJDT Parameters	Parameter
Raster	Program
Dehydrated Air	Carrier gas
3000	Sheath Pressure (sccm)
1350	Vacuum Pressure (sccm)
1500	Atomizer Pressure (sccm)
-23.2	z-height
100	Print speed (mm/sec)
0.25	y-spacing (mm)
60	# of passes

Table 13: AJDT Parameters for LSCF layer

4. Results & Discussion

4.1 Viscosity Measurements

Inks were characterized using an Anton Paar Rheolab QC to measure viscosity. Ink stability is not directly influential of fuel cell performance but will affect the AJDT technique used to fabricate the fuel cell. Viscosity affects the printability and shelf life of the ink. A less viscous ink would be more likely to atomize sufficiently during deposition. A spinning steel tip measured the viscosity in mPa•s at different shear rates. Thirty viscosity measurements were taken over shear rates ranging from 0 to 1300 1/s.
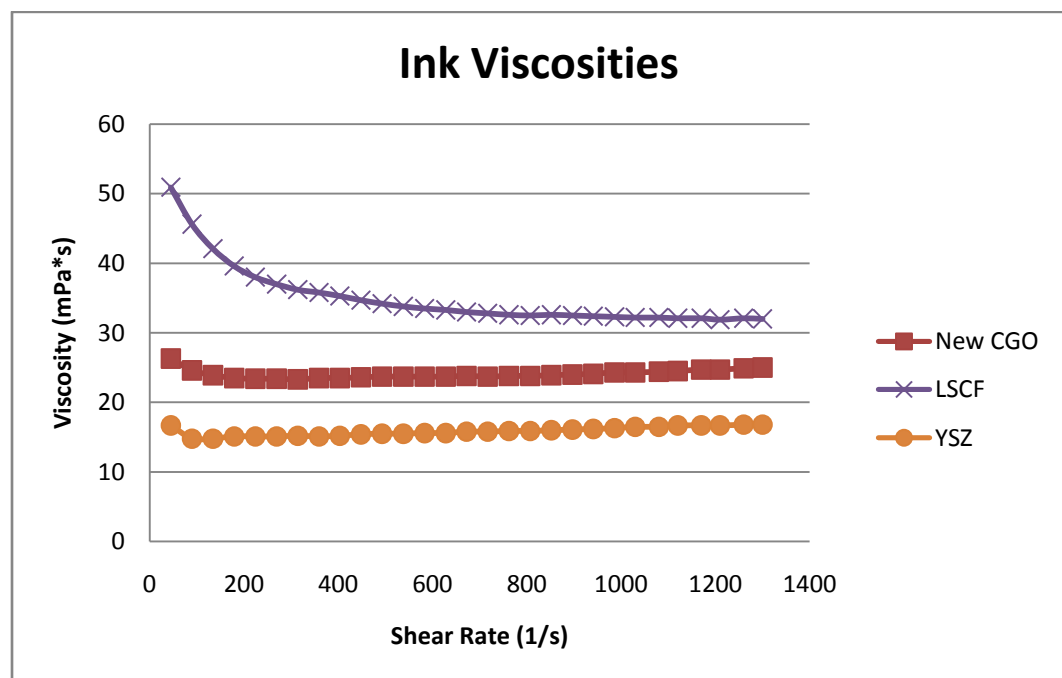

Fig. 11: Viscosities for the three types of inks used in fuel cell fabrication.

The viscosity measurements of the YSZ electrolyte, CGO buffer, and LSCF cathode inks can be seen in Fig. 11. The viscosity of the YSZ ink was approximately 15 mPa•s, the viscosity of the CGO ink was approximately 24 mPa•s, and the viscosity of the LSCF ink was approximately 32 mPa•s at high shear rates. Most of the inks formulated within this study were shown to possess viscosities that were relatively constant under varying shear rates. The ink that stood out was the LSCF cathode ink which showed non-Newtonian, shear thinning behavior.

Although higher viscosity inks may have particles in suspension longer, it can also reduce printability by clogging the AJDT's nozzle more rapidly. The printability of the YSZ electrolyte ink has been observed to be useable for the AJDT technique for approximately 2 weeks after formulation, under constant mixing conditions, whereas the other two inks require further optimization through additional studies to achieve this level of stability.

The viscosity measurements for four LSCF cathode inks with different ethyl cellulose types are seen in Fig. 12. These inks have 4 mg LSCF and are identical to one another except the ethyl cellulose type used as the binder additive. A progressive trend can be seen, with a direct correlation between ethyl cellulose intrinsic viscosity and the final ink viscosity. The ethyl cellulose (Y) ink which had a slightly lower viscosity than the ethyl cellulose 300 ink.
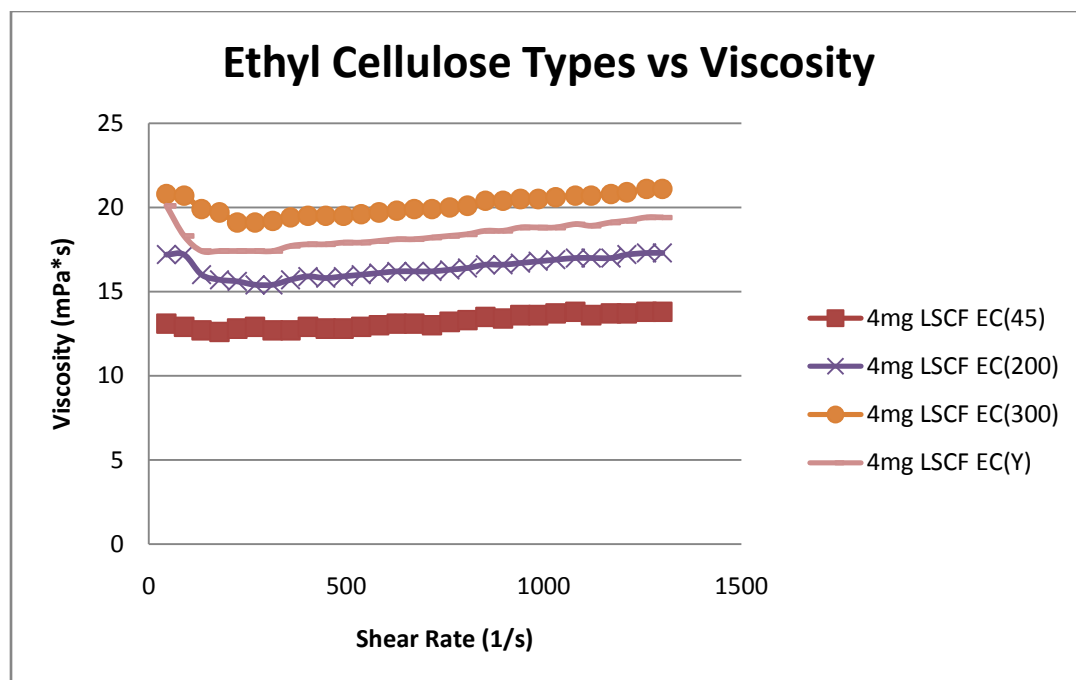
Fig. 12: Viscosity versus shear rate for the four types of ethyl cellulose.

4.2 Hydrodynamic Diameter

Dynamic light scattering (DLS) was performed on the four LSCF inks made with 4 mg LSCF to measure the hydrodynamic diameter of the inks. The hydrodynamic diameter is measured with the DLS technique which observes the diffusion of particles moving under Brownian motion and then converts this into a size distribution using the Stokes-Einstein equation. Different ethyl cellulose chain lengths should coat the particles differently and this will be evident in the hydrodynamic diameter measurements. The results of the dynamic light scattering measurements can be seen in Fig. 13 and Table 14. For ethyl cellulose 45, ethyl cellulose 200, and ethyl cellulose 300, the trend is progressive with a direct correlation between hydrodynamic diameter and ethyl cellulose size. However, for ethyl cellulose (Y), the hydrodynamic diameter is almost the same size of ethyl cellulose 45. Steric effects between the particles are a quantification of one

41

portion of the stability of the inks. The steric hindrance may be higher in inks with ethyl cellulose 200 or ethyl cellulose 300 and may lead to greater ink stability than inks with ethyl cellulose 45 or ethyl cellulose (Y). However, the substitution of these ethyl cellulose types alone was not sufficient to significantly prolong ink stability in LSCF cathode inks and further study would be required to determine what stability enhancement would be attained for each individual ink type.
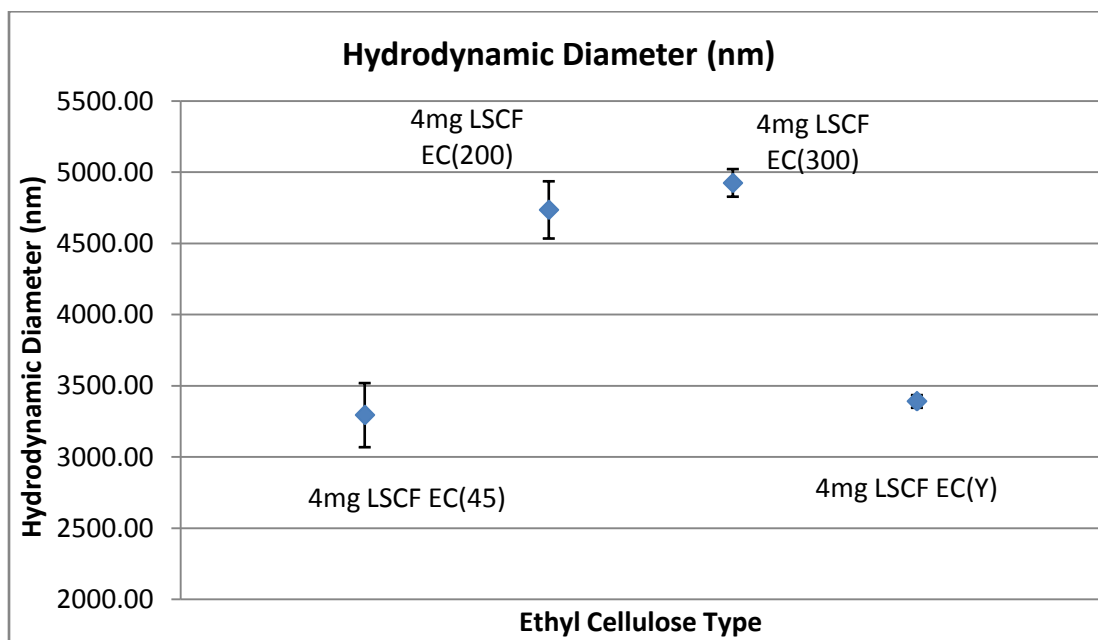

Fig. 13: Hydrodynamic diameter for the four inks with ethyl cellulose types

Sample	Hydrodynamic Diameter (nm)	Stdev
4mg LSCF EC45	3294	225
4mg LSCF EC200	4736	200
4mg LSCF EC300	4925	96
4mg LSCF EC(Y)	3390	44

Table 14: Hydrodynamic diameter for the four inks with ethyl cellulose types

4.3 Gel Permeation Chromatography

Different types of ethyl cellulose ink additives were analyzed using gel permeation chromatography (GPC), a common test to measure polymer structure, as seen in Table 15. This uses size exclusion to separate the analytes based on the polymer size. The results show the molecular weight, polydispersity index, and intrinsic viscosity of each ethyl cellulose type. The polydispersity index of a polymer is a measure of the distribution of molecular mass.

Ethyl Cellulose Type	Mw (daltons)	PI or Mw/Mn (daltons)	Intrinsic Viscosity (dL/g)	Mp in daltons (g/mol)
EC 45	51343	1.518	1.099	51015
EC 200	92438	1.473	1.6674	84017
EC 300	127210	3.142	2.0559	136244
EC (Y)	226980	1.478	1.6877	226980

Table 15: GPC results

The intrinsic viscosity from GPC analysis confirms the trend of viscosity versus ethyl cellulose type as observed from the rheometer results previously, as seen in Fig. 14. Again, ethyl cellulose size and viscosity were shown to be positively correlated except ethyl cellulose (Y) did not follow this trend. However, the intrinsic viscosity does not follow the hydrodynamic diameter trends but this may be attributed to the assumption within DLS of the particles being spherical.
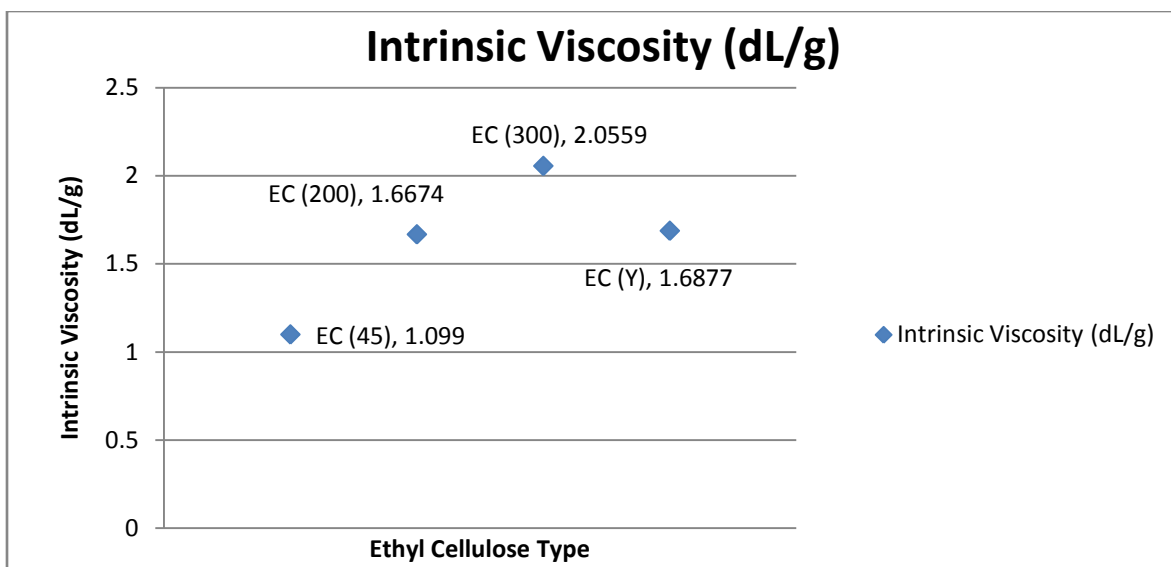
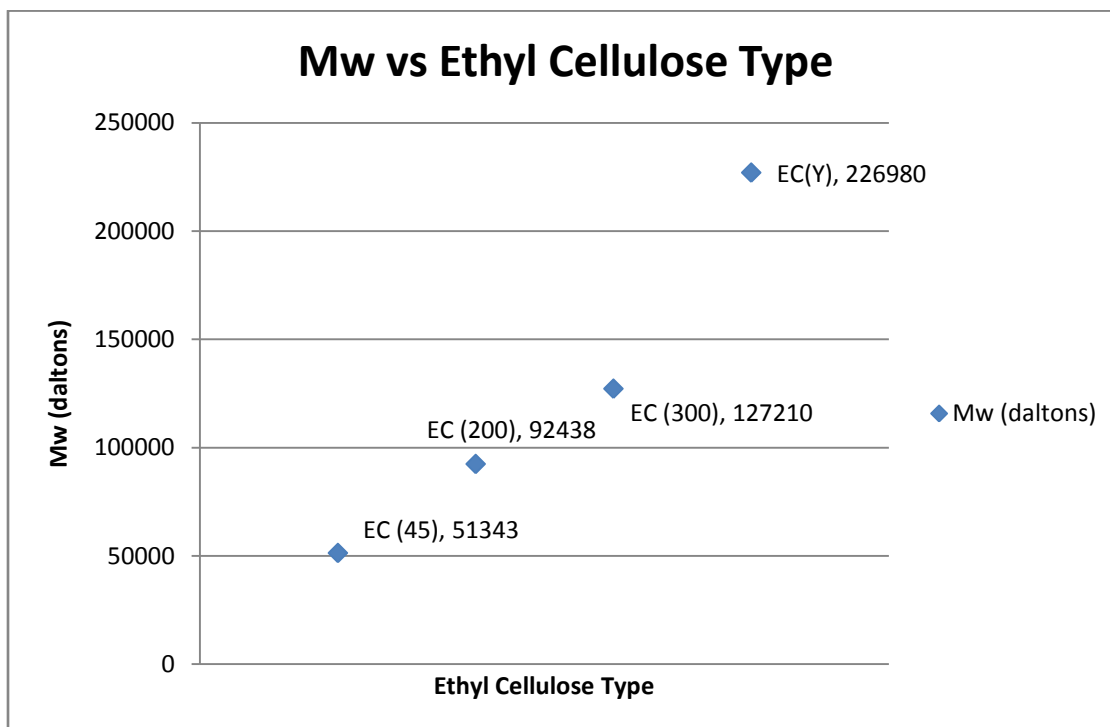Fig. 14: Intrinsic viscosity for the ethyl cellulose types

Fig. 15: Mw vs ethyl cellulose type

In Fig. 15, it is seen that the molecular weight of ethyl cellulose (Y) is the highest of the types of ethyl celluloses. This indicates that ethyl cellulose (Y) may possibly be a

more highly branched polymer than the others which would explain the decrease in viscosity while still having a higher molecular weight. Another possible explanation is it possesses a different ethoxy content. In fact, ethyl cellulose (Y) is more than twice the molecular weight of the next heaviest polymer and yet its intrinsic viscosity is lower.

4.4 Relationship Between Number of Passes and Thickness

The buffer and electrolyte layers should be designed to be thin to reduce resistance but sufficiently dense to prohibit gas diffusion between the two electrodes. The buffer layer was designed to be dense and approximately 5 microns thick after sintering, thus an experiment was devised to determine the number of passes required with the AJDT to produce this thickness with CGO. The LSCF cathode layer's thickness after sintering would be found in a similar manner.

The cells were broken into pieces and SEM images were taken of their cross-sections. ImageJ software was used to determine the average thickness of the CGO and LSCF layers after sintering. By knowing the distances between calibration points on the SEM image, the average thickness of the CGO and LSCF components could be determined. A relationship could then be devised between the number of passes of each component and the resulting layer thickness. The SEM images with calibration and thickness measurements are shown in Fig. 16. Fig. 16a is cross-section SEM at 5000x with the top layer being 24 passes of CGO and Fig. 16b is cross-section SEM at 5000x with the top layer being 24 passes of LSCF.
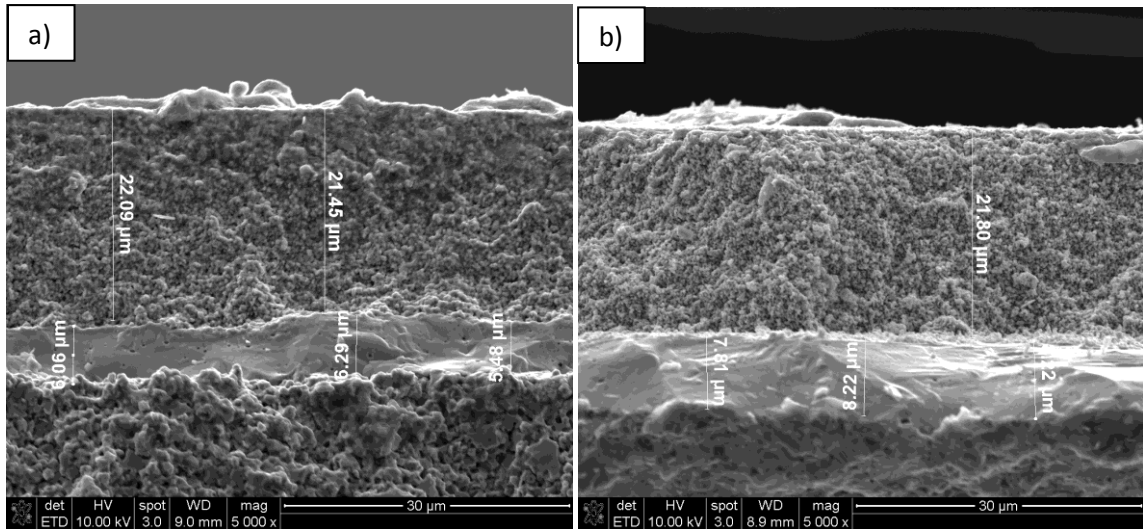
Fig. 16: SEM images for passes vs thickness experiment

After analyzing the SEM cross-section image of the fuel cell, it was calculated that 24 passes of CGO, at these settings, produced a dense layer of CGO, 22 microns thick. In order to produce a dense deposit of CGO 5 microns thick, 6 passes would be required. This number of layers of CGO was used throughout the experiment. A second calculation was made to determine the formula to convert from the number of passes with LSCF into the resulting LSCF deposit thickness. To produce 40 micron thick LSCF layer using 0.5mm y-spacing, 128 layers would be required. To produce 40 micron thick LSCF layer with 0.25mm y-spacing, approximately 60 layers would be required.

4.5 Preliminary Fuel Cell Fabrication Study and Baseline Experiment

The first identical pair of fuel cells was created with settings chosen to produce a dense microstructure, utilizing a shorter y-spacing and shorter z-height, to the substrate. The next identical pair of fuel cells was created with settings chosen to produce a very porous microstructure compared to the previous set, utilizing a wider y-spacing and

further z-height from the substrate. To compensate for less ink being deposited with this method, the number of layers had to be altered to produce a similarly thick cathode as the first set. The settings for the last identical pair were chosen to produce a microstructure in between the previous two pairs. The CGO layer was sintered at 1250 $^\circ$C for 2 hours.
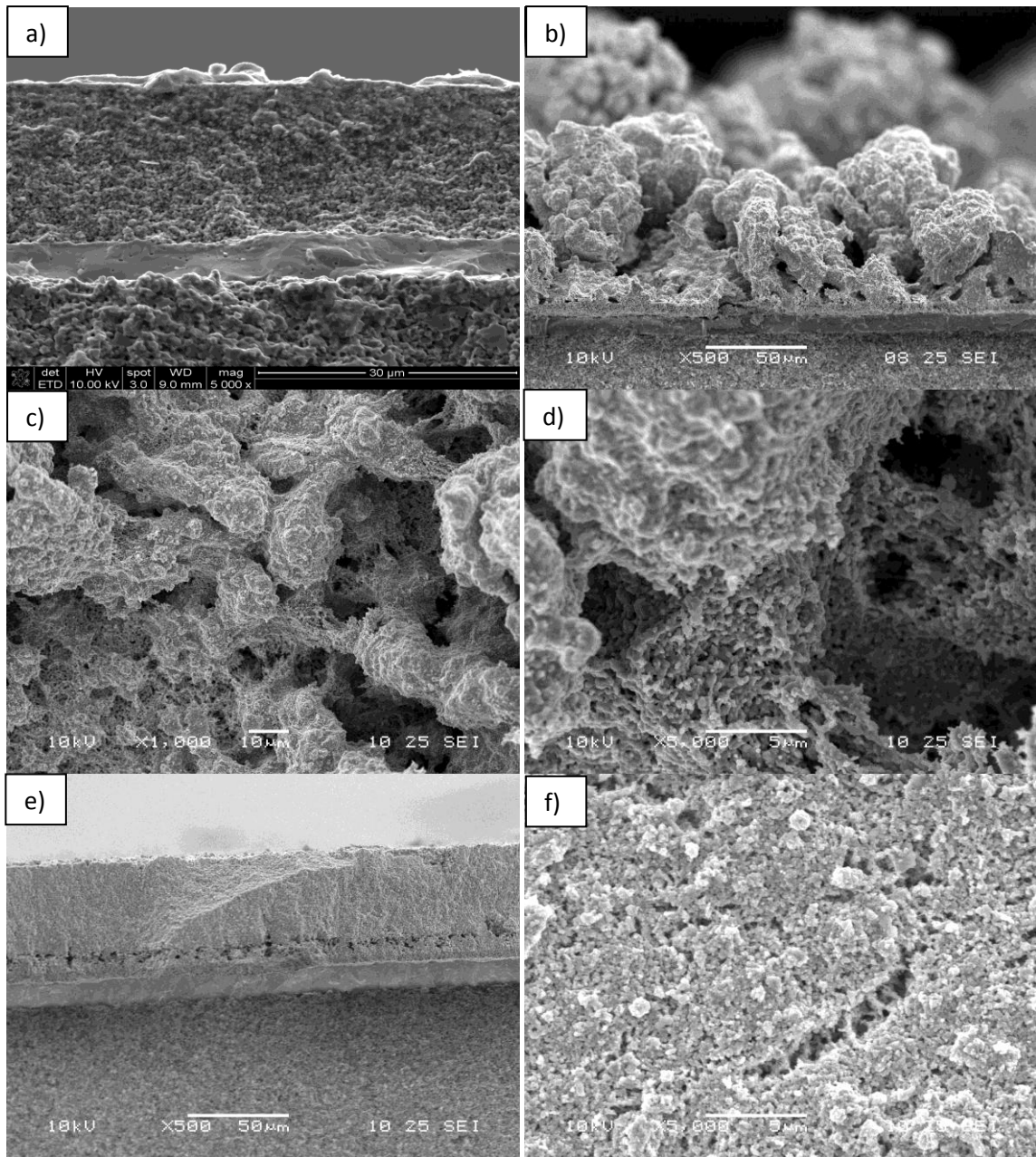

Fig. 17: Cross-section SEM images of AJDT experiment

The microstructures of the cathodes can be seen in SEM images shown in Fig. 17.

Fig. 17a is a cross-section SEM at 5000x of a fuel cell from pair #1 with AJDT

parameters with a dense microstructure, Fig. 17b is a cross section SEM at 500x of the

cathode with high porosity, Fig. 17c is a top-down SEM image at 1000x of the same

cathode, Fig. 17d is a top-down image at 5000x of the same cathode, Fig. 17e is a cross-

section SEM at 500x of the cathode with AJDT parameters with a density between the

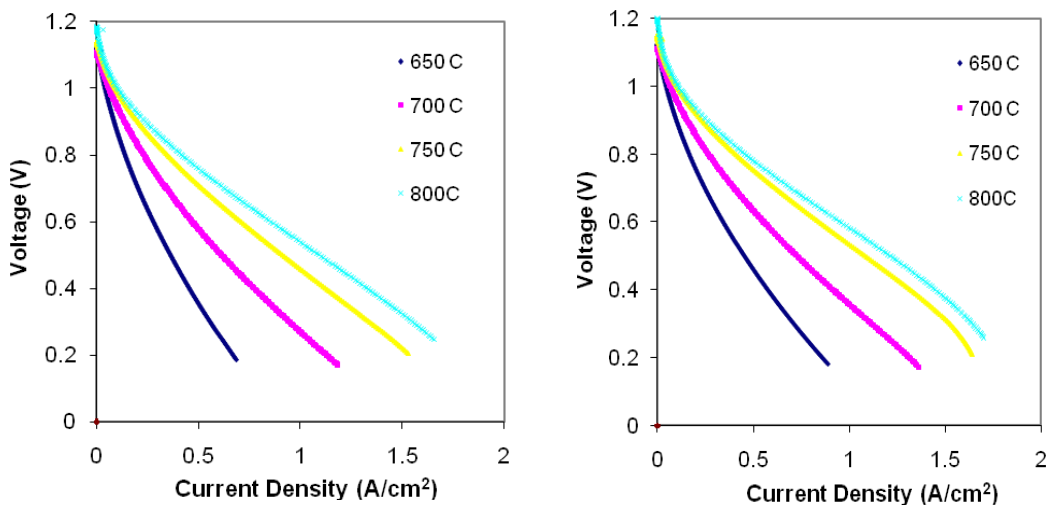first two pairs, and Fig. 17f is a top down SEM at 5000x of the same cathode.

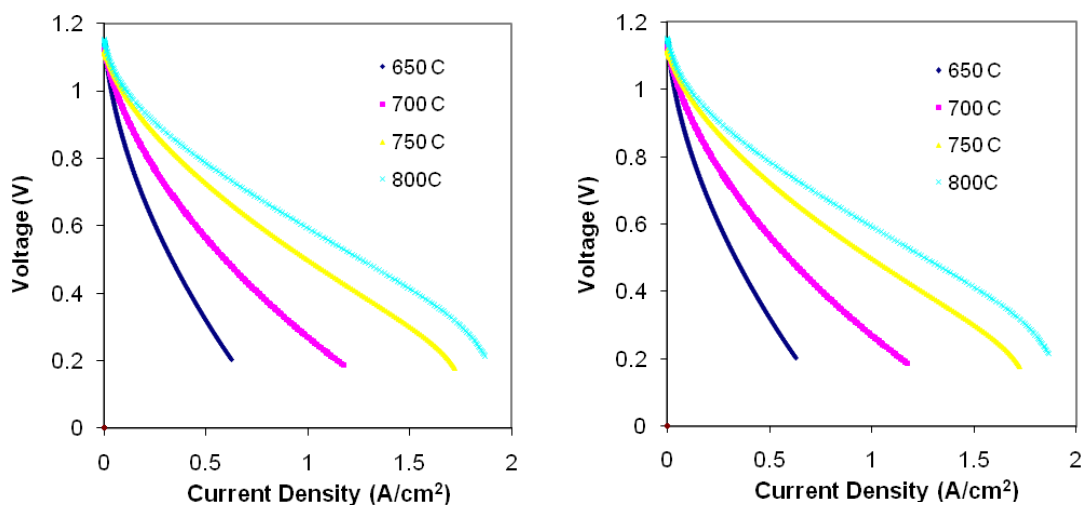Fig. 18: Polarization curves for fuel cell pair 1.

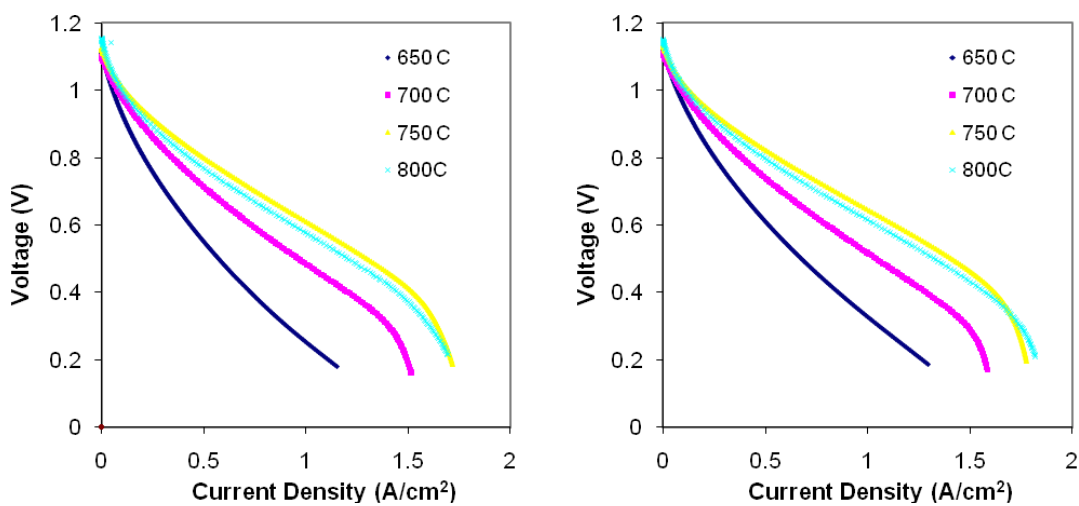Fig. 19: Polarization curves for fuel cell pair 2.

Fig. 20: Polarization curves for fuel cell pair 3.

The polarization curves can be seen in Figs. 18, 19, and 20. These three pairs of identical fuel cells were fabricated while altering multiple variables simultaneously so no exact comparison can be made between them, as far as polarization studies. The average current density for the first pair of fuel cells, which used AJDT parameters for a dense microstructure, was 1.67 A/cm². The average current density for the second pair of fuel

cells, which used variables to obtain a very porous microstructure, was 1.8 A/cm^2. This is an improvement of 8% in current density. The average current density for the third pair of fuel cells, which had a cathode microstructure with porosity in between that of the first two sets, was 1.71 A/cm^2.

However, the last set of fuel cells outperformed the fuel cell set with the most porous cathode at 700 °C, a lower operating temperature. This result correlates to the presence of a maximum in required porosity, above which any further increase in porosity reduces the amount of LSCF present, thereby decreasing active reaction sites and fuel cell current density. Nominally, porosity between 20-40% is desirable. (4)

An improvement at lower operating temperatures is the desired result. It may indicate possible use as an ITSOFC following further fuel cell optimization. An unusual horizontal feature within the cathode appears to have occurred in one of the fuel cells of the third pair. This fuel cell was examined with SEM imaging. The performance of this fuel cell was 1.68 A/cm^2 while its partner, of which the horizontal feature may not have occurred, had a current density of 1.81 A/cm^2. If the performance of the fuel cell with lower current density were removed from the average, these AJDT settings would prove to produce the best performance overall.

4.6 Experiment 1: Microstructure Change Due to Sintering

Four sets of identical pairs of fuel cells were fabricated using different sintering profiles to test the effect on the cathode microstructure. Next, SEM characterization was performed, as shown in Fig. 21, with ImageJ software to determine the cathodic microstructure changes created by using the different sintering temperatures. Fig. 21a is

a cross-section SEM image at 10000x magnification of a LSCF cathode sintered at 1020 °C, Fig. 21b is a cathode sintered at 1050 °C, Fig. 21c is a cathode sintered at 1080 °C, and Fig. 21d is a cathode sintered at 1120 °C.
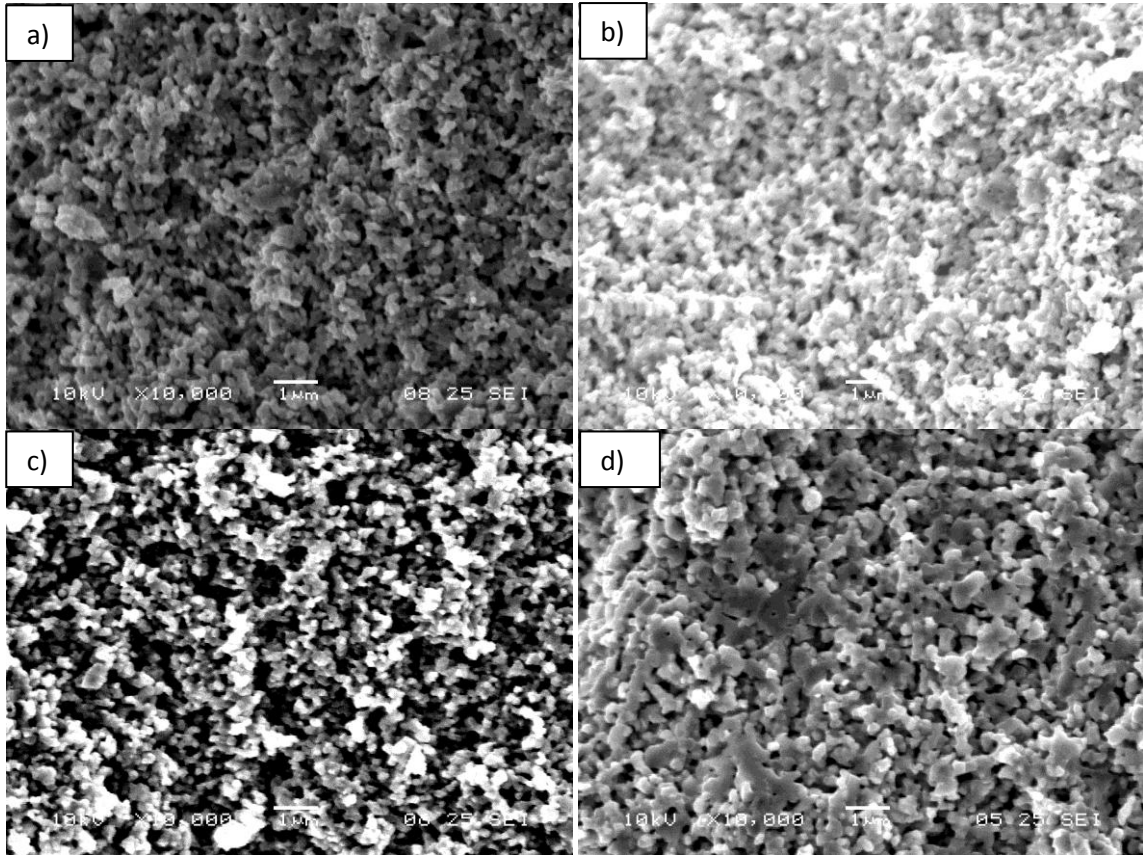

Fig. 21: Cross-section SEM images of sintering temperature experiment

Ten random grain samples were measured in parallel directions in each image to approximate the grain size of the specific cathode's microstructure, shown in Table 16. Smaller grain sizes and less densification would lead to higher surface area and more active reaction sites within the cathode. The overall trend is a positive correlation between grain size and cathode sintering temperature, with higher sintering temperatures producing larger grain size and denser microstructures. For instance, the cathode sintered at the highest temperature of 1120 °C had significant densification occur during sintering

and the largest grain sizes. A trend line was produced to show the mathematical

relationship between sintering temperature and grain size, as visible in Fig. 22. The

sintering temperature of 1020 °C produced a cathode microstructure with smaller grain

sizes, which would lead to higher surface area, and should be investigated further.

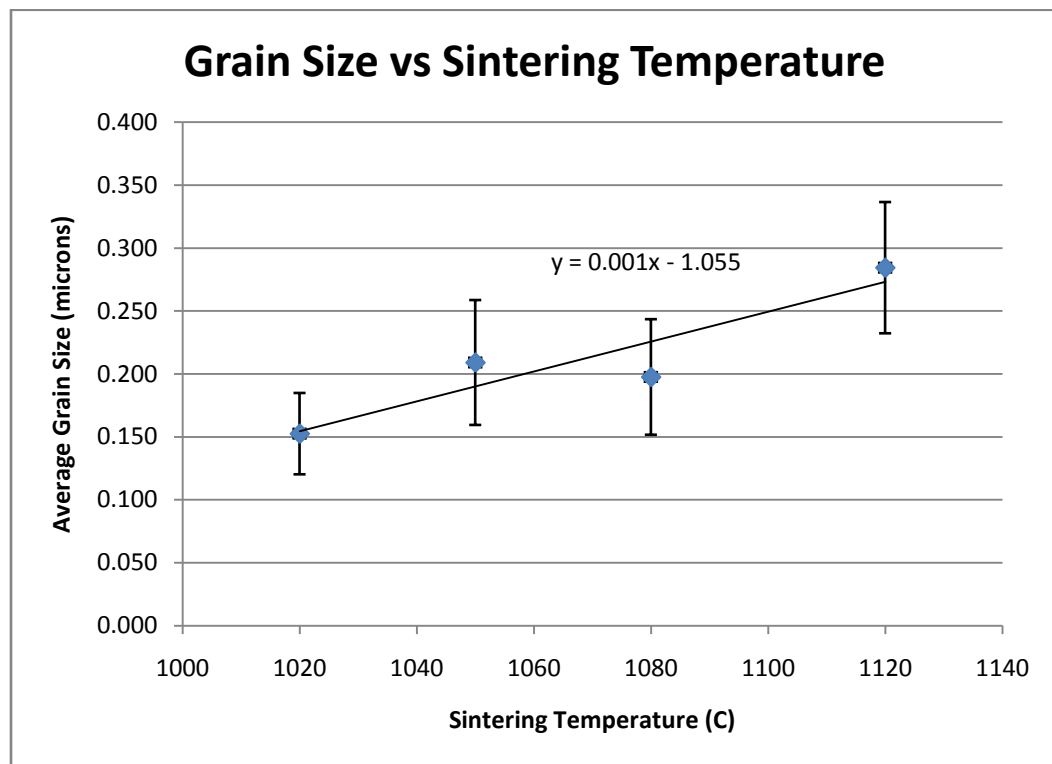| Temp (°C)	Avg grain size (microns)	Stdev grain size
1020	0.153	0.032
1050	0.209	0.050
1080	0.198	0.046
1120	0.284	0.052

Table 16: Grain size versus sintering temperature

Fig. 22: Grain size versus sintering temperature in LSCF cathode microstructures

4.7 Experiment 2: Microstructure Change Due to Binder

Three fuel cells were fabricated using different ethyl cellulose types as an ink additive to test its contribution to the cathode microstructure. The addition of ethyl cellulose to the ink can affect the viscosity and stability of the ink and can affect the porosity of the final sintered microstructure. The different ethyl cellulose types were: ethyl cellulose 45, ethyl cellulose 200, and ethyl cellulose (Y). These values were chosen to represent a range of ethyl cellulose types. SEM characterization was performed with ImageJ software to determine the cathodic microstructure changes created by using different ethyl cellulose types in the cathode inks alone. The effect the different ethyl cellulose types had on viscosity and hydrodynamic diameter were explored previously.

The cathode microstructure made with ethyl cellulose 45 has a higher porosity than the cathode made with ethyl cellulose 200 as seen in Fig. 23a and Fig. 23b, respectively. However, the cathode made with ethyl cellulose (Y) had a more porous microstructure as well, shown in Fig. 24. Combining these results with previous results from the GPC, there is a correlation between the hydrodynamic diameter associated with the ethyl cellulose type and the porosity of the resulting sintered cathode microstructure. If this is the case, then ethyl cellulose 45 and ethyl cellulose (Y) would provide a more advantageous cathode microstructure than either ethyl cellulose 200 or ethyl cellulose 300, due to the increased porosity created.
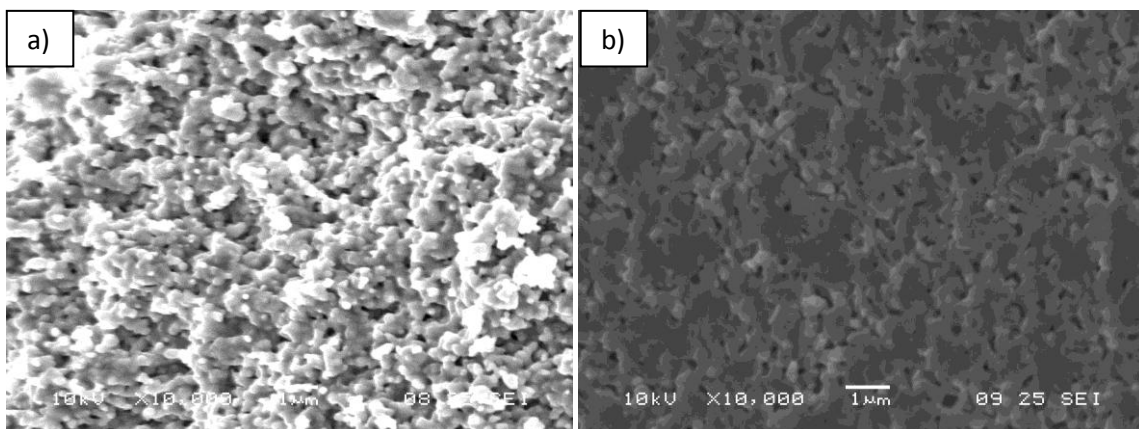
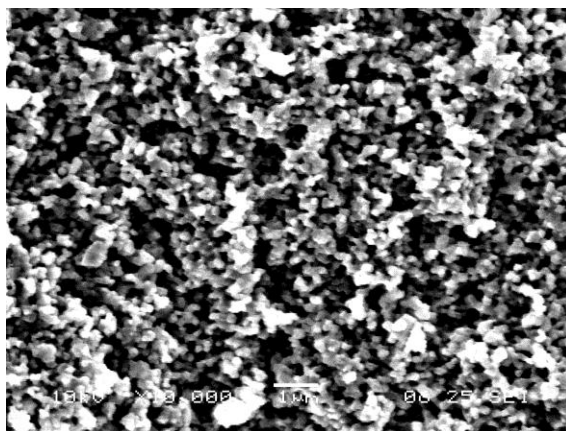Fig. 23: Cathode made with ethyl cellulose 45 and ethyl cellulose 200.

Fig. 24: Cross-section SEM of a cathode made with ethyl cellulose (Y)

Shorter chain length, higher order polymer branching, or a different ethoxy content appear to play a critical role in creating a microstructure with higher porosity. Conversely, for fuel cell layers that require a denser microstructure such as the electrolyte and buffer layers, the ethyl cellulose types with a longer chain length, less polymer branching, and the similar ethoxy content should be used.

5. Summary & Conclusions

The goal of this thesis was to formulate CGO buffer and LSCF cathode inks and determine parameters to be used for the novel Aerosol Jet Deposition Technique for fabricating fuel cells to enhance performance. This work is the first time solid oxide fuel cells with LSCF cathodes have been fabricated with this method. Inks were successfully formulated, characterized, and deposited onto anode substrates.

Multiple examinations were conducted to find the influence of multiple variables on the LSCF cathode microstructure. The polarization curves showed an 8% current density improvement through changing the baseline sets of parameters but optimizing these further should lead to increased performance. The polarization curves also showed a 19% improvement in current density when using LSCF as the cathode against a comparable LSM cathode based fuel cell. The set of AJDT parameters used in fuel cell pair 3 showed promise as a favorable intermediary between excess porosity of fuel cell pair 2 and the dense microstructure of fuel cell pair 1. Further study of fuel cell pair 2 and 3 and the gradient of parameters between them could be conducted to more precisely locate the optimum porosity of the microstructure for LSCF cathodes.

The next variable tested was sintering temperature and its effect on the cathode. The sintering temperature had a significant impact on microstructure but not as extensive as altering AJDT parameters. Cathode grain size was shown to change by 85% over the sintering temperatures examined. Higher sintering temperatures led to densification of the microstructure and lower surface area. This effect would be detrimental to fuel cell performance as it will diminish active reaction sites used for oxygen reduction. The

cathode sintered at 1020 °C would be expected to have the greatest current density but further studies would be required to confirm this hypothesis. A porous microstructure is beneficial since it leads to a higher active surface area, thereby increasing the reaction sites for oxygen reduction and increasing current density.

Lastly, the effect that the ethyl cellulose additive had on the resulting cathode was determined. This additive is a key component of the ink whose effects are multifaceted. The ethyl cellulose additive affects viscosity and stability of the ink and the porosity of the final microstructure. It was discovered that the porosity of the microstructure was not correlated to the additive's molecular weight. The actual causes of the cathode porosity may be the order of polymer branching or the ethoxy content of the ethyl cellulose. Shorter chain length, higher order polymer branching, or altered ethoxy content creates a LSCF cathode microstructure with higher porosity. These requirements would encompass ethyl cellulose 45 and ethyl cellulose (Y). Conversely, for fuel cell layers that require a denser microstructure such as the electrolyte and buffer layers, the ethyl cellulose types with a longer chain length, less polymer branching, and similar ethoxy content should be used. These requirements would encompass ethyl cellulose 200 and ethyl cellulose 300.

The ethyl cellulose was also investigated to examine its effect on ink viscosity and stability. The stability of the LSCF inks was not significantly impacted by altering the chain length of the ethyl cellulose binder; however the hydrodynamic radius did provide an indication of improved steric hindrance. The other component of stability, surface charge or zeta potential, requires investigation to stabilize the inks in this manner.

Additionally, other solvents could be examined external of the terpineol and 2-butanol solution used solely in this experiment.

The aerosol jet deposition technique has been shown to be an advantageous method of creating intermediate temperature solid oxide fuel cells of diverse microstructures, possibly paving the way for a wider range of fuel cell fabrication. This is the first time LSCF cathodes have been fabricated in combination with the AJDT technique. The fuel cells fabricated in this experiment show improved performance at lower temperatures than comparable fuel cells made with an LSM cathode. This should allow for more cost effective interconnects and fuel cell materials to be used in conjunction with fuel cells fabricated with this technique.

6. Future Outlook

The LSCF and CGO inks require further optimization to improve printability, stability, and fuel cell performance. The ink additives such as ethyl cellulose could be altered to fine tune the inks. One possibility is the use of alternate binders such as methyl cellulose which has smaller repeating monomers than ethyl cellulose and a lower intrinsic viscosity, which this study has shown to be beneficial in the resulting sintered microstructure of the cathode. Another avenue is solvent studies other than terpineol and 2-butanol.

Further studies of the AJDT parameters will also allow for finer control of the fuel cell microstructure. The set of AJDT parameters used in fuel cell pair 3 showed promise as a favorable intermediary between excess porosity of fuel cell pair 2 and the dense microstructure of fuel cell pair 1. Further study of fuel cell pair 2 and 3 and the gradient of parameters between them could be conducted to more precisely locate the optimum porosity of the microstructure for LSCF cathodes. Current density improvements much greater than 8% can be gained through further experimentation of LSCF cathode inks in conjunction with the AJDT fuel cell fabrication method.

7. References

1. **Srinivasan, Supramaniam.** *Fuel Cells: From Fundamentals to Applications.* New York City, New York : Springer Press, 2006.

2. **Huang, Kevin and Goodenough, John.** *Solid Oxide Fuel Cell Technology: Principles, Performance, and Operations.* Boca Raton, Florida : CRC Press, 2009.

3. **Sukeshini, Mary.** *Aerosol Jet Printing and Microstructure of SOFC Electrolyte and Cathode Layers.*

4. **Larminie, James.** *Fuel Cell Systems Explained.* s.l. : Wiley, 2003.

5. **Rose, Bob.** Engineers Forum On Sustainability: Fuel Cell Update. s.l. : US Fuel Cell Council, 2007.

6. **Hamann, Carl.** *Electrochemistry.* s.l. : Wiley, 2008.

7. **Hirschenhofer, J.H.** *Fuel Cell Handbook, Fourth Edition.* Reading, PA : Parsons Corporation, 1998.

8. **Howell, Thomas.** *Double Perovskite Materials for use as Sulfur Tolerant Anodes in SOFCs.* 2010.

9. **Dong, X. and Chen, Frank.** *LSGM As a Potential Anode Material for Intermediate Temperature All-Perovskite Solid Oxide Fuel Cells.* Daytona Beach, FL : s.n., 2010.

10. **Do, Anh-Tuan.** *Electrochemical Investigation of LSGMC-Composite Cathodes on LSGM-Substrate.* s.l. : The Electrochemical Society, 2008. Vol. 13.

11. **Hunsom, Mali.** *Investigation of La0.8Sr0.2CoO3/Ce0.85Sm0.15O2- x cathode performance of solid oxide fuel cell by electrochemical impedance spectroscopy: Effect of firing temperature.* 2006.

12. **Jiang, S. P.** *A comparison of O2 reduction reactions on porous (La,Sr)MnO3 and (La,Sr)(Co,Fe)O3 electrodes.* 2002.